EUROFUSION WPPFC-CP(16) 15188

A Kreter et al.

Overview of recent plasma-material interaction studies in the linear plasma device PSI-2

Preprint of Paper to be submitted for publication in
Proceedings of 26th IAEA Fusion Energy Conference

This work has been carried out within the framework of the EUROfusion Consortium and has received funding from the Euratom research and training programme 2014-2018 under grant agreement No 633053. The views and opinions expressed herein do not necessarily reflect those of the European Commission.

Overview of recent plasma-material interaction studies in the linear plasma device PSI-2

A. Kreter[1], M. Berger[1], D. Borodin[1], T. Dittmar[1], A.A. Eksaeva[2], A. Huber[1], S. Kraus[1], Y. Martynova[1], S. Möller[1], D. Nicolai[1], A. Pospieszczyk[1], M. Rasinski[1], M. Reinhart[1], T. Schlummer[1], B. Schweer[1], G. Sergienko[1], I.A. Sorokin[2], I. Steudel[1], A. Terra[1], B. Unterberg[1], M. Vogel[1], K. von Bovert[1], M. Wirtz[1], Y. Yuan[3] and Ch. Linsmeier[1]

[1]Forschungszentrum Jülich GmbH, Institut für Energie- und Klimaforschung, Partner of the Trilateral Euregio Cluster (TEC), 52425 Jülich, Germany

[2]National Research Nuclear University MEPhI, 31, Kashirskoe sh., 115409, Moscow, Russia

[3]School of Physics and Nuclear Energy Engineering, Beihang University, 100191 Beijing, China

E-mail contact of main author: a.kreter@fz-juelich.de

Abstract. This contribution summarizes the recent plasma-material interaction studies on the linear plasma device PSI-2 focusing on the topics of fuel retention, erosion and evolution of surface morphology of metallic materials. The aim of these studies is the qualification of plasma-facing materials proposed for future fusion reactors: tungsten and reduced activation ferritic martensitic (RAFM) steels. Depending on individual tasks, material samples were exposed either to pure deuterium or noble gas or mixed species plasma. The fraction of impurities such as helium, argon or nitrogen added to deuterium plasma was controlled by optical emission spectroscopy and in-situ mass analyzer. Exposure parameters were an electron density of ~10^{17}-10^{19} m^{-3}, an electron temperature of 3-20 eV, an ion flux to the target of ~10^{21}-10^{23} $m^{-2}s^{-1}$ and an incident ion energy of 20-300 eV, controlled by the target biasing. The sample temperature can be controlled in a range between 400-1400 K, covering the values for different first wall regions in a reactor. The incident ion fluence can be varied in a range between ~10^{23}-10^{27} m^{-2} by extending the duration of exposure. A Nd:YAG laser (lambda = 1064 nm) with a maximal energy per pulse of 32 J and a duration of 1 ms was used to apply repetitive heat loads for the ELM simulation on material samples. Optical emission spectroscopy (OES), target mass-loss technique and recently installed in-situ quartz microbalance (QMB) were employed to quantify the amount of eroded material. The deuterium retention was investigated by thermal desorption spectrometry (TDS) and nuclear reaction analysis (NRA). Scanning electron microscopy (SEM) including focused ion beam (FIB) cross-sectioning and transmission electron microscopy (TEM) was used to observe the evolution of the surface morphology.

1. Introduction

The fuel retention and the lifetime of plasma-facing components are critical factors potentially limiting the availability of a magnetic fusion reactor. Currently, tungsten is the main candidate as the plasma-facing material in a reactor. Reduced activation ferritic martensitic (RAFM) steels are considered as a cheaper and technologically less challenging solution for the main chamber wall. Even with the fully metallic first wall, the fusion fuel can be retained, e.g. by the co-deposition or in-bulk retention in metals. Under the bombardment by plasma particles the plasma-facing materials are eroded, thus limiting the lifetime of the first wall components.

The first wall in ITER will be subjected to mixed species fluxes containing hydrogenic isotopes (H/D/T), helium produced in D-T reactions and radiator gases such as argon, neon or nitrogen applied for a redistribution of power from the divertor plasma to a larger surface

area. It is necessary to test how plasma-facing materials perform with respect to hydrogen retention and erosion under the mixed species plasma conditions.

Linear plasma devices are excellent test beds for investigating specific questions of plasma-material interaction (PMI). The materials can be tested under well-defined plasma exposure conditions relevant to fusion edge plasma. This contribution summarizes recent PMI studies on the linear plasma device PSI-2 [1]. PSI-2 was originally installed and operated at the Humboldt University in Berlin [2]. In 2009 it was moved to Forschungszentrum Jülich to serve as a pilot experiment for the JULE-PSI project [3], which foresees a linear plasma device in the nuclear environment for testing neutron irradiated materials. The JULE-PSI device is by now in an advance stage of design and construction. Therefore, PSI-2 is now focusses on reactor relevant PMI studies.

2. Experimental

PSI-2 is a linear plasma device [1] with a steady-state magnetic field of 0.1 T and a plasma diameter of 6 cm. Samples of a typical lateral size of 5-20 mm and a few mm thickness were manufactured of tungsten and RAFM steels. Depending on individual tasks, material samples were exposed either to pure deuterium or noble gas or mixed species plasma. The fraction of impurities such as helium, argon or nitrogen added to deuterium plasma was controlled by optical emission spectroscopy and in-situ mass analyzer. Exposure parameters were an electron density of $\sim 10^{17}$-10^{19} m^{-3}, an electron temperature of 3-20 eV, an ion flux to the target of $\sim 10^{21}$-10^{23} $m^{-2}s^{-1}$ and an incident ion energy of 20-300 eV, controlled by the target biasing. The sample temperature can be controlled in a range between 400-1400 K, covering the values for different first wall regions in a reactor. The incident ion fluence can be varied in a range between $\sim 10^{23}$-10^{27} m^{-2} by extending the duration of exposure. A Nd:YAG laser (λ =1064 nm) with a maximal energy per pulse of 32 J and a duration of 1 ms was used to apply repetitive heat loads for the ELM simulation on material samples. Optical emission spectroscopy (OES), target mass-loss technique and recently installed in-situ quartz microbalance (QMB) were employed to quantify the amount of eroded material. The deuterium retention was investigated by thermal desorption spectrometry (TDS) and nuclear reaction analysis (NRA). Scanning electron microscopy (SEM) including focused ion beam (FIB) cross-sectioning and transmission electron microscopy (TEM) was used to observe the evolution of the surface morphology.

3. Results

3.1.Erosion of tungsten

The linear plasma device PSI-2 is equipped with an imaging optical emission spectroscopy (OES) system for in-situ measurements of sputtering. However, the calculations converting the number of photons measured by OES to the number of eroded particles suffer from the uncertainties in atomic databases and are strongly dependent on the local plasma parameters and experimental geometry. In contrast, the in-situ quartz microbalance (QMB) system recently installed on PSI-2 detects directly the particles sputtered from the target and transported to QMB. However, also for QMB a model for the interpretation of the measurements is necessary, i.e. for the calculation of the loss fraction of eroded particles on the way to the detector. The mass loss technique measures the amount of eroded material by the comparison of the sample mass before and after the exposure. The method, however, lacks the time resolution and therefore requires stable exposure parameters. While OES is sensitive to gross erosion, QMB and mass loss measure the net fraction of erosion.

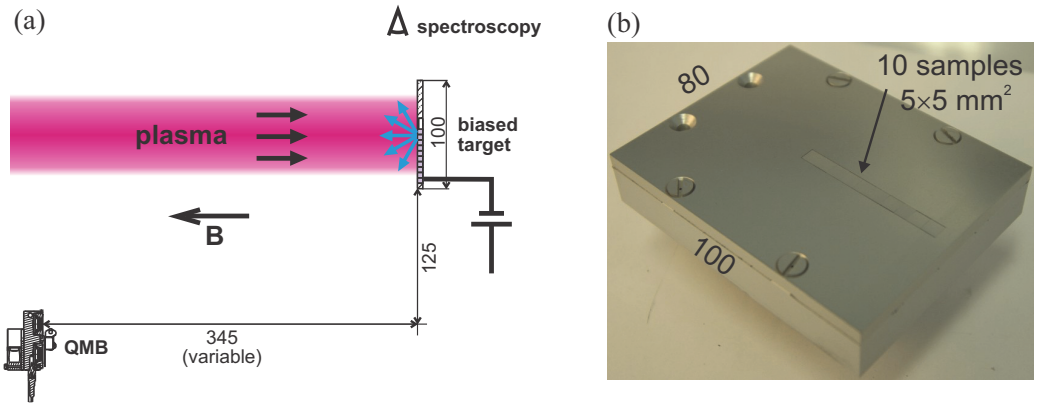

FIG. 1. Set-up of the experiment on tungsten erosion. (a) geometry of the experiment, (b) tungsten target with samples for mass loss measurements.

In the set of experiments described here, QMB, OES and the mass loss technique were simultaneously used to measure tungsten sputtering by argon and neon plasmas. The experiment was designed to provide a consistent set of data for the interpretation by the numerical code ERO [4]. A bulk W target covered the entire diameter of the plasma column of 6 cm (FIG.1). A set of ten 5×5 mm^2 W samples was incorporated in the target providing radially resolved mass loss data. The measurements were performed under the variation of the discharge power between 0.8 - 3.6 kW, incident ion flux 0.6 - 3.2×10^{21} $m^{-2}s^{-1}$ and incident ion energy 40 - 150 eV, below and above the W sputtering threshold. The angular distribution of sputtered W was determined by the variation of the target position with respect to QMB. The fraction of double charged ions, measured by an in-situ mass analyser [5], was of a few percent, except for the case of argon plasma with a power of 3.6 kW, where it reached 28%. The surface morphology after the experiment was observed by scanning electron microscopy.

FIG.2(a) shows the results of mass loss for the low power case and an incident neon ion energy of 140 eV. The radial profile of the mass loss corresponds to the hollow profile of the incident ion flux typical for PSI-2 [1]. In FIG.2(b) these data are compared with the predictions by the TRIM code [6], which uses the binary collision approximation (BCA). Generally, there is a good agreement between the experiment and the TRIM code calculations. FIG.3 shows W deposition rates measured by QMB for different fluxes of neon ions as a function of the incident ion energy. The deposition rates increase with the incident

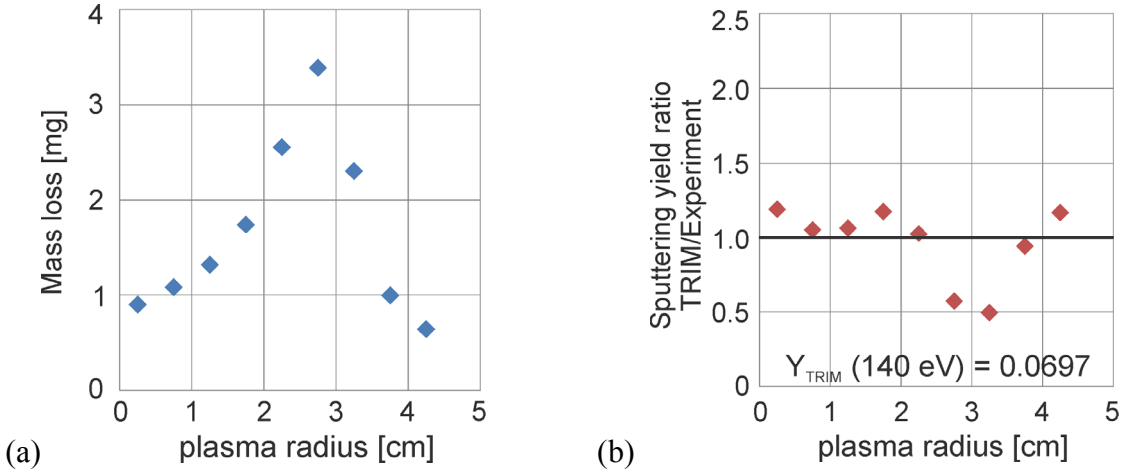

FIG. 2. Mass loss measurements for neon plasma, low power case, incident ion energy 140 eV. (a) radial distribution, (b) ratios to the value predicted by TRIM for the conditions.

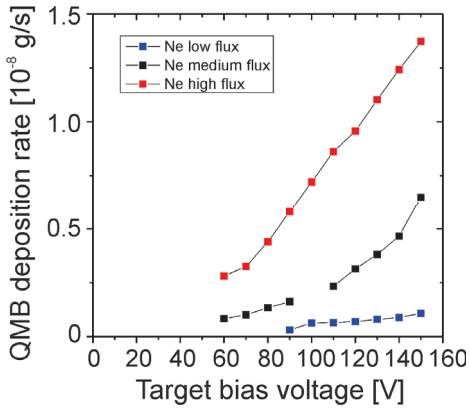

FIG. 3. Deposition on QMB as a function of bias voltage for different incident ion fluxes

flux and ion energy, in agreement with TRIM. The ERO code was used to evaluate the W sputtering rates from the QMB data [4]. The data were also used to match the measurements by spectroscopy.

3.2. Influence of impurities on erosion, fuel retention and outgassing of tungsten

The influence of helium, argon, neon and nitrogen on the deuterium retention in tungsten was investigated in under mixed plasma conditions in the linear plasma device PSI-2 [7]. Tungsten samples were mechanically polished, then recrystallized at 1800°C for 1 h before the exposure in PSI-2. The exposure conditions were as follows: incident ion flux of ~10^{22} $m^{-2}s^{-1}$, incident ion fluence of $5x10^{25}$ m^{-2}, sample temperature of 500 K, incident ion energy of 70 eV. Following mixed plasmas were produced: pure D, D+He (3%), D+Ar (7%), D+Ne (10%) and D+N (~5%). The fraction of impurities was controlled by spectroscopy except for N, where it was estimated from the puffing rates.

FIG.4 shows SEM images of sample surfaces after exposure. In the case of pure D, two main groups of blisters were observed: large (few μm size) and small (few 100 nm size). Blistering depends on the grain orientation. There are grains with large and small blisters, only small blisters and with reduced blistering. Small blisters can grow on the top of large ones. Many blisters are open, small holes close to the bases of blisters are visible in SEM. For these samples exposed to pure D plasma, it was not possible to obtain information on the W grain orientation by the Electron Backscatter Diffraction (EBSD) technique, because the signal was too blurry presumably due to many defects in the near surface area.

Samples exposed to D+He plasma were only ones with a smooth surface appearance by "naked eye" after the exposure. All other samples were visibly rough, probably due to large blisters. In the D+He case, blisters have reduced density and are less developed. It is known from previous experiments at similar plasma conditions that 3% He reduces the D retention by a factor of ~2-3. Exclusively to the sample exposed to D+He plasma, a nano-size structure on the entire surface was observed by high-magnification SEM, which can be associated with

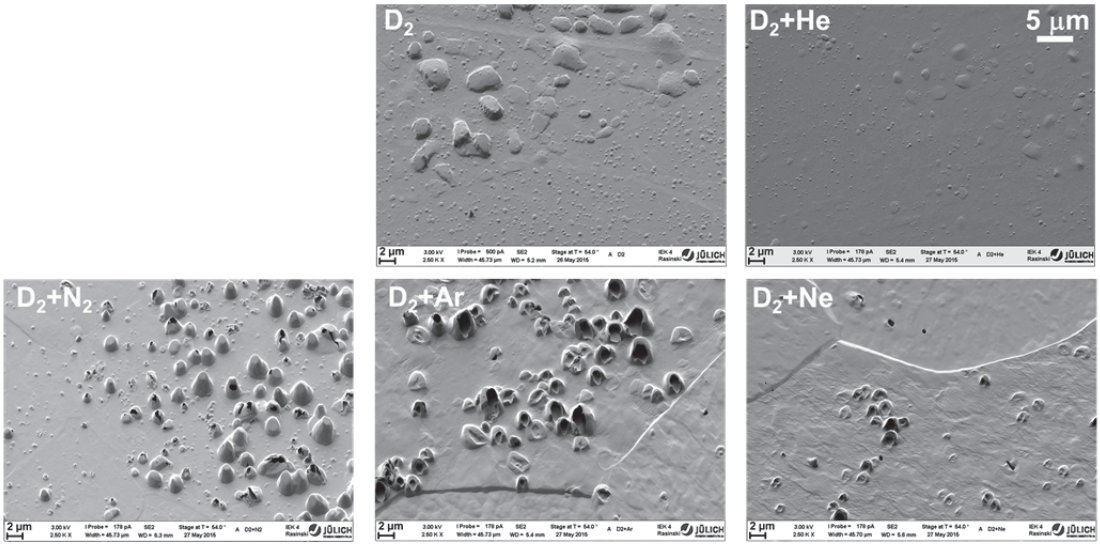

FIG. 4. SEM images of the surface morphology of tungsten samples after plasma exposure

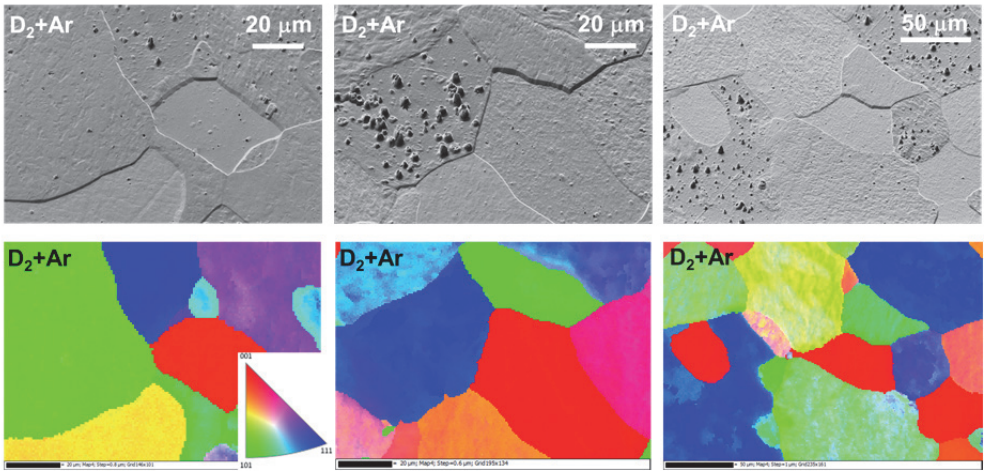

FIG. 5. SEM and EBSD images of the sample exposed to D-Ar plasma

He nano-bubbles protruding to the surface.

In the D+Ar case, as for pure D, blistering depends on the grain orientation. However, in the D+Ar case we were able to perform EBSD (FIG.5), because the number of surface defects was less than for the pure D case. Grains oriented 111 showed the strongest blistering. Also the sputtering depends on the grain orientation, with 001 grains showing the strongest sputtering. The difference in sputtering yields between grains is up to ~$5*10^{-3}$, which corresponds to ~30% of the sputtering yield for Ar on W calculated by TRIM for these conditions. Almost all blisters are corrupted after the exposure. Blisters at different stages of erosion are visible. There are no (or very few) "growing" blisters visible. Therefore, assuming that blisters grow continuously in the course of exposure, blisters must pop up on a fast time scale. The D+Ne case is similar to D+Ar: most of blisters are corrupted and strongly eroded; different sputtering rates are observed for different grains.

Samples exposed to D+N plasma have a somewhat similar appearance as for D+Ar and D+Ne, but less pronounced erosion effects for blisters and different grains. This is probably due to the lower sputtering yield of W by N. There are large blisters with a cone-like shape, protruding significantly higher than those for pure D, which are rather "flat".

It is known from previous TEM investigations, that helium forms an open porosity network of nano-bubbles for 20-30 nm depth in tungsten. This porous layer can locally store a high amount of hydrogen. It also provides pathways for hydrogen, which then, once recombined, can travel fast to the surface and escape. Therefore, the He layer effectively serves as a diffusion barrier for implanted hydrogen, thus decreasing the H retention.

Argon and neon, by sputtering, keep a low number of defects in the near-surface layer of tungsten exposed to mixed plasmas. The effect of nitrogen seems to lie between helium on one side and argon/neon the other side. Some additional defects are introduced by N (less than by He), and not sputtered away as efficiently as by Ar/Ne.

The Ne seeding reduced the D retention by a factor of ~3-6, also when, in addition to plasma exposure, successive and simultaneous transient heat loads were applied.

Dynamic outgassing following the exposure of tungsten to pure D, D+He and D+N plasmas was investigated for different sample temperatures [8]. Two faraday-mode quadrupole mass spectrometers were used to distinguish D, He and N outgassing from the samples. FIG.6 shows the outgassing curves for the pure D exposure for different target temperatures and fluences. The outgassing rate follows the t^{α} power law with $\alpha = -0.96 \pm 0.1$ for the D and

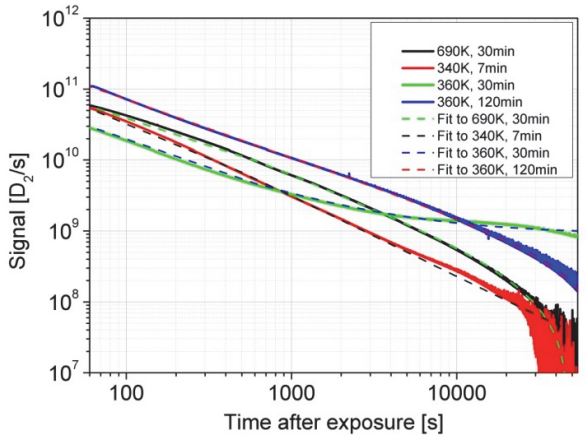

FIG. 6. Outgassing of W targets after exposure at conditions as described in the legend

D+He cases. The He outgassing is lower and drops below the detection limit 2 min after the exposure, while the D outgassing is observable for at least 24 hours.

3.3. Performance of tungsten: synergies in power and particle loads

Synergistic effects of simultaneous and sequential deuterium plasma and ELM-like transient heat loads on the fuel retention and surface morphology of tungsten were investigated [9]. An increase in the D retention by a factor of 12 was observed during the simultaneous plasma and transient heat loads. Exposures to first transient heat loads and then plasma showed an increased D content by a factor of 3.6 in comparison to the pure plasma loading. This can be attributed to the enhanced D clustering by the thermal shock exposures, increased mobility of D along the shock-induced cracks as well as increased diffusion of D into the W material caused by strong temperature gradients during the laser pulse exposure.

Combined particle (hydrogen and helium) and pulsed high heat load exposures (up to 10^6 pulses) of tungsten were performed [10,11]. A detailed post-mortem analysis of the obtained results exhibited a complex interconnection between the thermally and the (H/He) particle induced surface modifications (FIG.7). The formation of blisters was strongly reduced or even suppressed due to the surface temperature rise during a transient event. He induced nanostructures were strongly modified in terms of height and agglomeration of tungsten filaments. Apart from that, the H and He particle exposures altered the mechanical and thermal properties of the materials due to embrittlement and the formation of near surface nano bubbles. Furthermore, recrystallisation of the material, which will take place especially during long term operation, will additionally deteriorate the mechanical strength of the PFM. The combination of these effects will make the material more prone to thermal shock and fatigue damages such as crack formation, surface roughening due to plastic deformation and

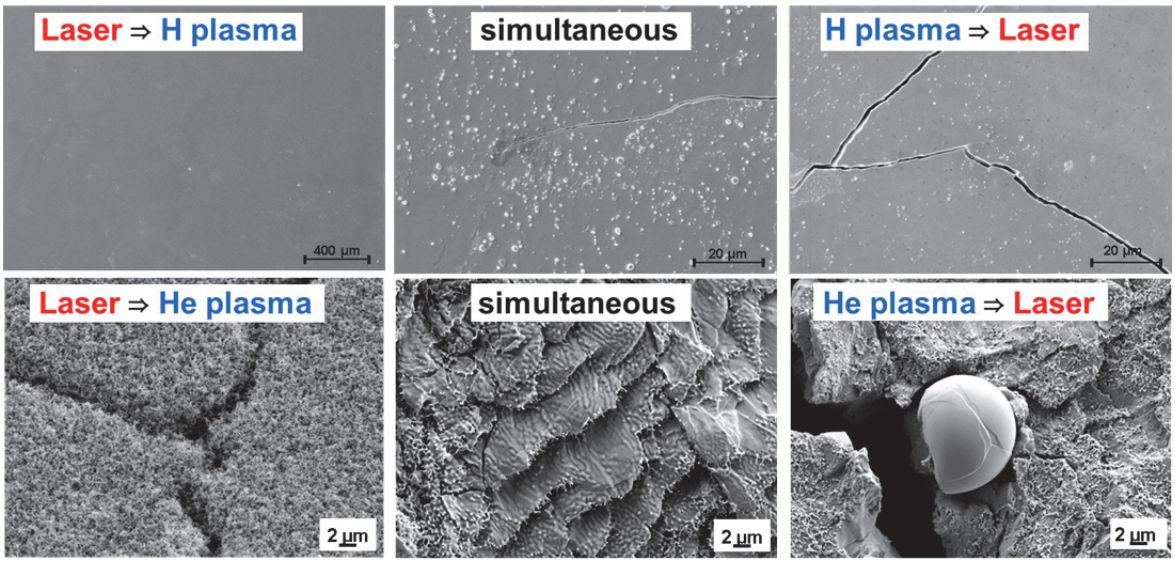

FIG. 7. SEM images of tungsten after sequential and simultaneous exposure to plasma and ELM like heat loads. Upper row: hydrogen plasma, bottom row: helium plasma.

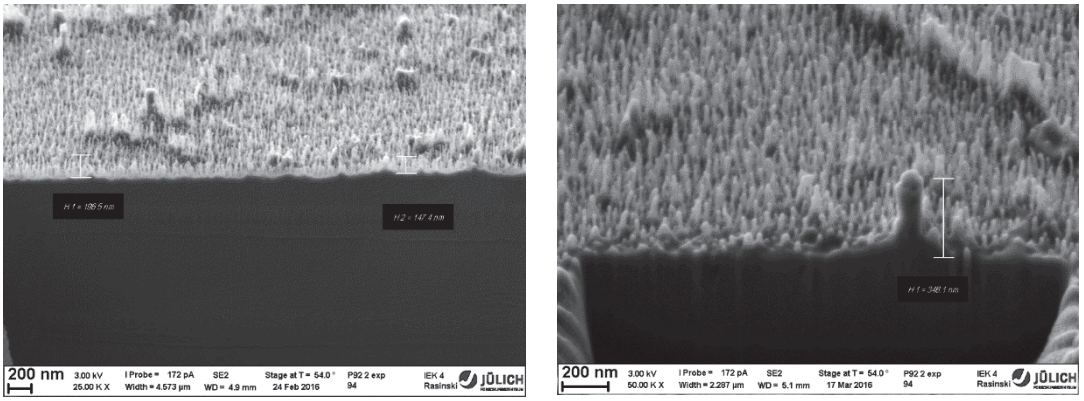

FIG. 8. Typical SEM images of P92 steel after exposure to D plasma. Eurofer 97 exhibits similar behaviour.

the formation of molten material on the plasma facing surface. The simultaneous high heat load and particle exposure showed that fuzz and bubble formation are not only formed on the surface but also inside the induced cracks. This will also enhance the risk of material erosion.

3.4.Performance of reduced activation ferritic martensitic steels

RAFM steels of the Eurofer 97 and P92 grades with 1.06 and 1.75 wt.% W (0.3 and 0.5 at.%) and polycrystalline W and Fe as reference materials were simultaneously exposed to D plasma at sample temperatures below 450 K and fluences of $\geq 10^{26}$ D/m^2 [12] As documented by SEM after all plasma exposures both steels (FIG.8) and iron samples demonstrated similarly highly eroded and porous surface microstructure. Introduction of helium by mixed exposures (with 5 and 10 % He) to deuterium plasma intensified the sputtering process of steel and iron samples. RAFM steels showed a lowering of sputtering in the course of exposure to deuterium plasma. This is attributed to the surface enrichment by W, confirmed by the surface analysis.

The D retention in Eurofer 97 and P92 steels was 10-15 times lower than in W, which can be attributed to a faster deuterium diffusion and lower density of strong trapping sites in steels.

The evolution of surface morphology of P92 pre-exposed to disruption- and ELM-like heat loads was investigated for simultaneous and sequential D plasma and laser induced transient heat loads [13]. There was no connection between the loading sequence and the surface modifications for the disruption preloaded samples. On the contrary, the ELM preloaded samples exhibited surface roughening, melting and the formation of holes dependent on the loading sequence and power density.

4. Summary

The JULE-PSI project foresees a linear plasma device in the nuclear environment for plasma-material interaction with neutron irradiated and toxic materials. The linear plasma device PSI-2 served as pilot experiment for JULE-PSI project, but now focuses on reactor relevant PMI studies. The experimental studies focus on (i) the qualification of tungsten as plasma facing material including erosion, evolution of surface morphology and thermo-mechanical properties, the fuel retention and outgassing, including the influence of plasma impurities; (ii) the qualification of RAFM steels (e.g. Eurofer 97) as a candidate material for main chamber wall in DEMO; (iii) combined effects of particle and heat loads on plasma-facing materials. The ERO code was adapted for PSI-2 and benchmarked with experiments on W erosion.

Acknowledgements

This work has been carried out within the framework of the EUROfusion Consortium and has received funding from the Euratom research and training programme 2014-2018 under grant agreement No 633053. The views and opinions expressed herein do not necessarily reflect those of the European Commission.

References

[1] KRETER, A., et al., "Linear plasma device PSI-2 for plasma-material interaction studies", Fusion Sci. Technol. **68** (2015) 8.

[2] KORNEJEW, P., et al., "Chemical Erosion of CFC at High Ion Flux Densities", Phys. Scr. **T91** (2001) 29.

[3] UNTERBERG, B., et al., "New Linear Plasma Devices in the Trilateral Euregio Cluster for an Integrated Approach to Plasma Surface Interactions in Fusion Reactors", Fusion Eng. Des. **86** (2011) 1797.

[4] EKSAEVA, A.A., et al., "ERO modelling of tungsten erosion in the linear plasma device PSI-2", Nucl. Mater. Energy, submitted.

[5] SOROKIN, I.A., et al., "In-situ mass-spectrometer of magnetized plasmas", Nucl. Mater. Energy, submitted.

[6] ECKSTEIN, W., Calculated sputtering, reflection and range values, IPP report, IPP 9/132 (2002).

[7] RASINSKI, M., et al., "The microstructure of tungsten exposed to D plasma with different impurities", Nucl. Mater. Energy, submitted.

[8] MÖLLER, S., et al., "Dynamic outgassing of deuterium, helium and nitrogen from plasma-facing materials under DEMO relevant conditions", Nucl. Mater. Energy, submitted.

[9] HUBER, A., et al., "Deuterium retention in tungsten under combined high cycle ELM-like heat loads and steady-state plasma exposure", Nucl. Mater. Energy, in print, http://dx.doi.org/10.1016/j.nme.2016.04.007.

[10] WIRTZ, M., et al., "Impact of combined hydrogen plasma and transient heat loads on the performance of tungsten as plasma facing material", Nucl. Fusion **55** (2015) 123017.

[11] WIRTZ, M., et al., "Influence of helium induced nanostructures on the thermal shock performance of tungsten", Nucl. Mater. Energy, in print, http://dx.doi.org/10.1016/j.nme.2016.07.002.

[12] MARTYNOVA, Y., et al., "Deuterium retention in RAFM steels after high fluence plasma exposure", Nucl. Mater. Energy, submitted.

[13] STEUDEL, I., et al., "Melt-layer formation on PFMs and the consequences for the material performance", Nucl. Mater. Energy, in print, http://dx.doi.org/10.1016/j.nme.2016.08.002.